Research Article

Controlled 90° domain wall motion in $BaTiO_3$ piezoelectric ceramics modified with acceptor ions localized near grain boundaries

Akira Miyaura[1] · Taiki Kawaguchi[1] · Manabu Hagiwara[1] · Shinobu Fujihara[1]

Abstract
The irreversible motion of non-180° ferroelectric domain walls is a predominant cause for the increased hysteretic loss in piezoelectric ceramics at elevated temperatures. In this study we designed piezoelectric ceramics modified with acceptor ions localized near grain boundaries for the purpose of suppressing the irreversible domain wall motion at elevated temperatures without diminishing the contribution from the reversible domain wall motion. Particles of undoped $BaTiO_3$ (BT) were coated with Mn-doped BT by a coprecipitation method and then sintered to form a Mn-modified BT ceramic. Structural and dielectric characterizations indicated that the Mn ions in the resulting ceramic were localized near grain boundaries. The measurement of the unipolar electric-field-induced strain was conducted for the Mn-modified and unmodified (pure) BT ceramics at temperatures up to 120 °C (just below the Currie temperature) to discuss the hysteretic behavior in their piezoelectric response. The results showed that the effective piezoelectric coefficient d^*_{33} of the Mn-modified BT ceramic was comparable to the unmodified BT ceramic. The hysteresis of the Mn-modified BT ceramic was retained below 40% in the whole temperature range whereas that of the unmodified BT ceramic increased significantly at elevated temperatures over 100 °C. The results in this study demonstrate that the localized Mn ions effectively pin the domain walls to suppress their irreversible motion at elevated temperatures, while the reversible motion inside the grains remains possible.

Keywords Piezoelectric ceramics · Barium titanate · Domain wall · Chemical modification

1 Introduction

Motion of non-180° ferroelectric domain walls under an externally applied electric or stress field is an important factor affecting the dielectric, mechanical, and electromechanical properties of piezoelectric ceramics [1–4]. Domain walls move across a potential energy landscape randomly disturbed by point defects and/or defect dipoles [3, 5]. Such a domain wall motion is usually categorized into reversible and irreversible motions: a domain wall moves reversibly in a potential well under a small field, whereas it overcomes potential barriers to move irreversibly when a sufficiently large field is applied. The latter irreversible motion drastically enhances the magnitude of piezoelectric response, but simultaneously it causes hysteretic behavior to the external fields, leading to increased energy loss during operation [6, 7]. The increased hysteretic loss due to the irreversible domain wall motion can lead to unstable operation and heating of piezoelectric devices [8, 9]. The contribution of the irreversible domain wall motion is known to become more obvious at elevated temperatures because thermal energy makes the potential wells less efficient for pinning the wall [3].

Recently, development of piezoelectric materials applicable to high-temperature operation has been required in many application areas such as actuators for a fuel injector in automobiles [10]. Piezoelectric ceramics for the high-temperature actuator applications are usually evaluated

✉ Manabu Hagiwara, hagiwara@applc.keio.ac.jp | [1]Department of Applied Chemistry, Faculty of Science and Technology, Keio University, 3-14-1 Hiyoshi, Kohoku-ku, Yokohama 223-8522, Japan.

SN Applied Sciences (2019) 1:286 | https://doi.org/10.1007/s42452-019-0304-z

Received: 25 December 2018 / Accepted: 25 February 2019 / Published online: 2 March 2019

by their longitudinal piezoelectric coefficient (d_{33}) and their Curie temperature (T_C) or depolarization temperature. Based on this perspective, for example, $BiScO_3$–$PbTiO_3$ (BS–PT) solid solution is regarded as a promising material for this application due to its high d_{33} (460 pC/N) and high T_C (450 °C) [11]. The applicability of piezoelectric ceramics to the high-temperature actuators, however, also depends on their hysteretic behaviors at elevated temperatures. Actually, the literature has shown that the strain (*S*)—electric field (*E*) curve of a BS–PT ceramic becomes significantly hysteretic at a high temperature over 300 °C although this temperature is well below its T_C [12]. The usage of BS–PT for the actuator application is thus limited within relatively narrow temperature range despite its high T_C. This example shows that the control of the irreversible domain wall motion at elevated temperatures is essentially important for the development of piezoelectric ceramics for high-temperature actuator applications.

The contribution of the domain wall motions in piezoelectric ceramics is usually controlled via doping of acceptor or donor ions [13]. When acceptor ions [e.g., Fe^{3+} in $PbZr_{1-x}Ti_xO_3$ (PZT)] are doped, oxygen vacancies are formed to maintain the net charge neutrality. That defect dipoles (or defect complexes) formed by the oxygen vacancy and the acceptor ion are aligned along the polarization direction of the unit cell to stabilize the domain walls [14]. As a result, the acceptor doping strongly pins the domain walls, making the ceramics "hard." The resultant hard piezoelectric ceramics with homogeneously dispersed acceptors show a linear *S*—*E* curve with a small hysteresis due to the decreased mobility of domain walls. However, the magnitude of piezoelectric strain (i.e., d_{33}) in such hard ceramics must be small because domain walls are pinned everywhere in individual grains, and the contribution from the reversible domain motion is also decreased. The conventional hard piezoelectric ceramics thus are not suitable for the actuator applications. In an opposite way, donor-doped soft piezoelectric ceramics (e.g., Nb^{5+}-doped PZT) show a lager piezoelectric response since domain walls in them are easy to move, but the hysteretic loss in them tends to increase significantly at elevated temperatures.

For the reasons stated above, it is required to develop a method to suppress the irreversible domain wall motion at elevated temperatures without inhibiting the reversible one. In order to achieve this, in this study we propose core–shell structured piezoelectric ceramics composed of grains with an undoped (soft) core and an acceptor-doped (hard) shell. In such ceramics, irreversible domain-wall motion is expected to be suppressed by defects localized near grain boundaries, while the walls are allowed to move reversibly by "bowing [15] " in the core. Barium titanate $BaTiO_3$ (BT) is chosen as a model piezoelectric material in this study, although its low T_C (~ 130 °C) is not suitable for high-temperature applications, because defect chemistry and domain wall structure in it have been well understood by previous studies. The Mn-doped BT shell supported on undoped BT particles were synthesized via a coprecipitation process and then sintered to form the core–shell BT ceramics composed of undoped core and Mn-doped shell (Fig. 1). Investigation of microstructure, crystal structure and electrical properties showed that Mn ions were successfully doped only near grain boundaries. Finally, we demonstrated that the increase in the hysteresis loss under unipolar driving ceramics in the core–shell BT was effectively suppressed at elevated temperatures compared to the unmodified (pure) BT ceramics.

2 Experimental procedure

2.1 Preparation of core–shell particles

A powder of undoped BT (BT-05, Sakai Chemicals Co., Ltd.; average particle size 0.5 μm) was used as the core particles. A shell of 2 mol% Mn-doped BT was formed on the core particles via a coprecipitation method by the following procedure. 0.480 mmol (117.3 mg) of $BaCl_2{\cdot}2H_2O$ (99.0%, Wako Chemicals Co., Ltd.), 0.392 mmol (0.0430 mL) of $TiCl_4$ (99.0%, Wako Chemicals Co., Ltd.), and 0.008 mmol

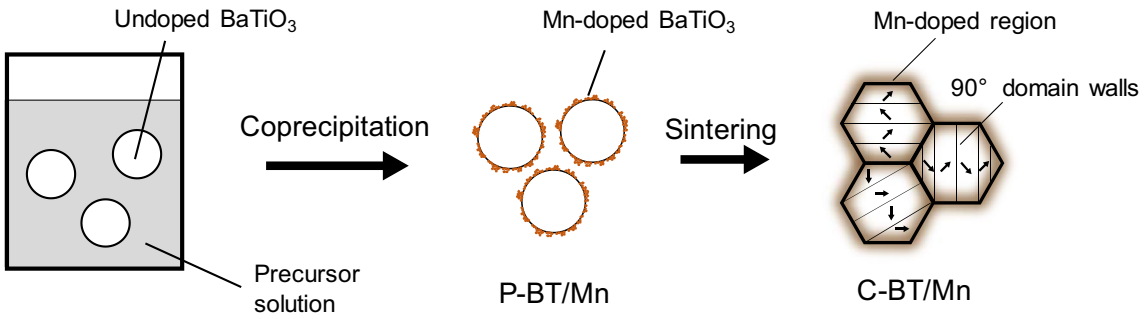

Fig. 1 A scheme for fabricating Mn-modified BT ceramics via a coprecipitation process

(1.6 mg) of $MnCl_2 \cdot nH_2O$ (99.0%, Wako Chemicals Co., Ltd.; $n = 0.871$) were added to 8 mL ion-exchange water to form a precursor solution. Separately, 27.4 mol (1.096 g) of NaOH was dissolved in 17 mL ion-exchange water, then 1 g BT-05 was added and stirred for 10 min under ultrasonication. The precursor solution was added drop wise to the BT-dispersing NaOH solution, then stirred for 30 min under ultrasonication. The resulting slurry was then kept at 90 °C under stirring for 4 h in an oil bath. Finally, the powder was collected by filtration and washed with NH_3 aqueous solution (pH 12) in order to prevent Ba-ion leaching [16], and vacuum-dried over 1 h and subsequently dried at 60 °C. The resulting powder with a Mn-doped BT shell is referred as P-BT/Mn.

2.2 Fabrication of sintered samples

To fabricate bulk ceramic samples, P-BT/Mn was mixed with 2 wt% of poly(vinyl acetate) and uniaxially pressed into pellets at 150 MPa for 1 min. The green pellets were heated to 700 °C and held for 2 h to remove the binder and then sintered in air at 1300 °C held for 30 min with a heating rate of 5 °C min^{-1}. The sintered sample prepared from P-BT/Mn is hereafter named as C-BT/Mn.

For comparison, a ceramic sample of unmodified BT was also fabricated. To reveal the effect of the Mn-doped shell layer on the domain wall mobility in C-BT/Mn ceramics, it is necessary to fabricate an unmodified BT ceramic with a similar grain size because grain size has a great impact on the domain wall contribution to the electrical properties of BT ceramics [17]. We found, however, that it was difficult to obtain well-densified unmodified BT ceramics with a similar grain size with C-BT/Mn (~ 0.5 µm) by sintering of the BT-05 powder. For this reason, we fabricated an unmodified BT ceramic by the following conventional solid-state reaction and the two-step sintering method [18] to achieve the small grain size around 0.5 µm. Stoichiometric amounts of $BaCO_3$ (99.9%, Kanto Chemical Co., Ltd.) and TiO_2 (99.9%, Kojundo Chemical Laboratory Co., Ltd) were ball milled for 24 h using ethanol and yttria-stabilized zirconia balls and then dried. The mixed raw powder was calcined at 1000 °C for 2 h, followed by ball milling for 24 h. The calcined powder was granulated and pressed in a similar way with P-BT/Mn. The green pellets were sintered by the two-step sintering method. In the two-step sintering process, the pellets were heated at 15 °C min^{-1} to a temperature of 1200 °C, then immediately cooled to a temperature of 1120 °C and held for 20 h. The obtained undoped BT ceramic is referred as C-BT. As a reference material to compare T_C and the room-temperature piezoelectric response, a ceramic of 0.5 mol% Mn-doped BT was also fabricated via the same conventional solid-state route.

2.3 Characterizations

The particle/grain size and morphology of the powder and ceramic samples were observed using a field-emission scanning electron microscope (FE-SEM; JSM-7600F, JEOL) in the secondary-electron mode. Prior to the FE-SEM observation of the ceramic samples, the surface of them was polished and thermally etched by a heat treatment at a temperature 50 °C lower than the sintering temperature for 10 min. Particles of P-BT/Mn were also observed by a field-emission scanning electron microscope (FE-TEM; TECNAI F20, Philips). For the observation of the domain structure of C-BT/Mn, the polished and thermally etched sample was chemically etched in $HCl:HF:H_2O = 1:1:100$ solution for 10 s. The etched surfaces were observed using another FE-SEM (Inspect F50, FEI). The phase and lattice parameters of the ceramic samples were determined by X-ray diffraction (XRD; D8-02 diffractometer, Bruker AXS) with Cu Kα radiation. For electrical characterizations, the sintered pellets were ground and electroded with Pt-conductive paste, and fired at 900 °C for 10 min in air. Temperature dependence of dielectric permittivity (ε_r) for the samples was measured from room temperature to 200 °C by applying a small AC voltage of 0.5 V_{p-p} at 1 kHz using an LCR meter (ZM2371, NF Corp.) in combination with a tube furnace. The ceramic samples with Pt electrodes were poled by applying a DC electric field in silicone oil at 100 °C for 30 min. The poling field was 2.0 kV mm^{-1} for C-BT and 4.0 kV mm^{-1} for C-BT/Mn. A higher poling electric field was needed for C-BT/Mn to align defect dipoles in the sample, whereas the field of 4.0 kV mm^{-1} was too high for C-BT because of its poorer electrical insulation property. Nevertheless, the poling field of 2.0 kV mm^{-1} is much higher than the coercive field (E_c) of undoped BT ceramics ($E_c < 0.5$ kV·mm^{-1} at room temperature) and thereby was enough to achieve full poling of C-BT. After the poling treatment, the samples are aged for 24 h at room temperature. The unipolar S–E curve of the poled samples was measured using a contact-type displacement sensor (Millimar C1216, Mahr) under applying a triangle wave of 0.1 Hz at varying temperatures between room temperature and 120 °C.

3 Results and discussion

Figure 2 shows FE-SEM images of particles in BT-05 (core) and P-BT/Mn. BT-05 has rounded particles with a smooth surface. After the coating of Mn-doped BT, the surface of the particles is observed to become rough while the overall morphology and size are not changed. The FE-TEM image of a particle of P-BT/Mn, shown as the inset of Fig. 2b, clearly shows that the most part of the surface of

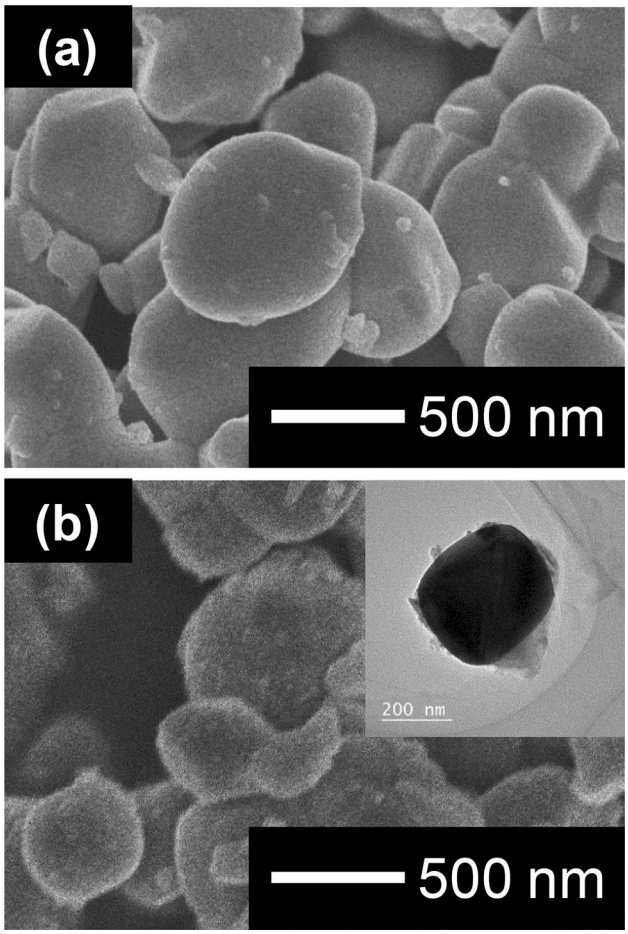

Fig. 2 FE-SEM images of **a** BT-05 and **b** P-BT/Mn. The inset image in (**b**) shows a result of an FE-TEM observation of a particle of P-BT/Mn

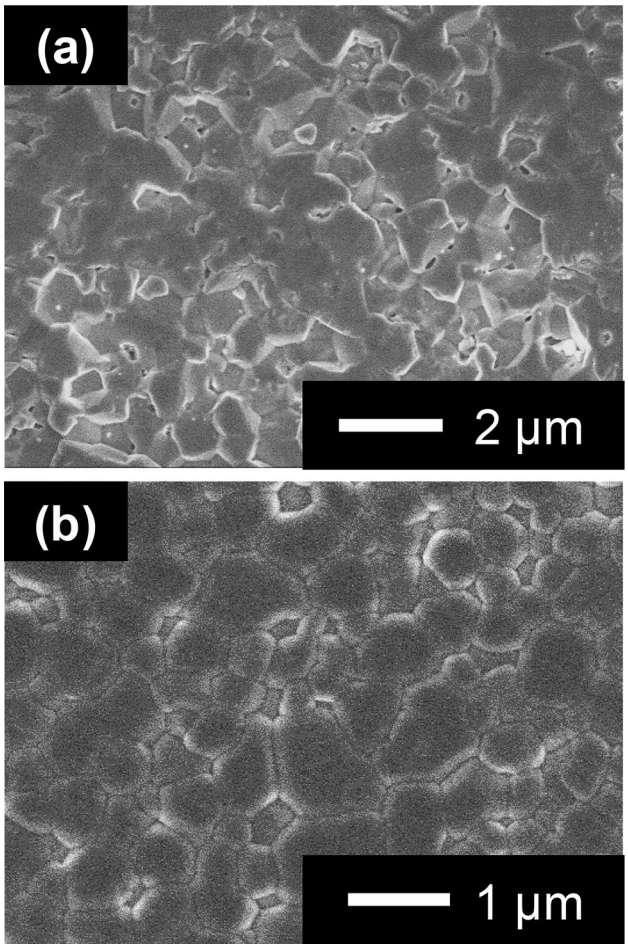

Fig. 3 FE-SEM images of the polished and etched surface of **a** C-BT and **b** C-BT/Mn

the core (black region) is covered with precipitates (dark gray region). The XRD measurement was unavailable to identify this shell region as the crystalline phase of Mn-doped BT due to the small fraction of the shell region in the sample and also due to overlapping of the peaks from the shell and core regions. However, we confirmed that a powder precipitated from the same precursor solution without the cores showed diffraction peaks assigned to the single-phase perovskite at slightly lower angles compared to the pure BT. This indicates that the precipitate from the solution is the crystalline phase of Mn-doped BT in which the larger Mn^{2+} ions (ionic radius $r = 83$ pm) substitute for the Ti^{4+} ions ($r = 61$ pm). Because the existence of the cores should not prevent the precipitation of Mn-doped BT from the solution, one can reasonably infer that the observed shell region in P-BT/Mn is the crystalline Mn-doped BT phase.

The ceramic sample fabricated from P-BT/Mn (i.e., C-BT/Mn) showed a brown color, which is attributed to optical absorption due to the d–d transition in the Mn ions, whereas the unmodified BT ceramic (C-BT) was white. Figure 3 shows FE-SEM images of the thermally etched surface of C-BT and C-BT/Mn. Both samples show a well-densified microstructure composed of fine grains around 0.5 μm. Relative density was as high as 95% for both samples. It is important to note that the grain size in C-BT/Mn is almost unchanged from P-BT/Mn, indicating that the grain growth, which is a result of matter transport across the grain boundary, does not occur during the sintering process. The suppressed grain growth in C-BT/Mn may relate to the doped Mn ions concentrated near grain boundary [19]. The densification without grain growth is critically important for retaining the Mn ions around the grain boundary.

The resulting fine grain size is also important for achieving the desired domain structure. It is known that the 90° domain structure in BT ceramics changes from the simple lamellar type to the so-called banded type with increasing grain size [20]. Within a grain having the banded structure, thin plates with lamellar domains are stacked each

other across 180° domain boundaries so as to cancel out the net polarization. Thus 90° domain walls in the banded structure does not extend directly from one side to the other of a grain. Such a domain structure does not serve the purpose of controlling the domain wall mobility using defects concentrated near the grain boundary. According to Arlt's estimation, the critical grain size separating the two types of domain structures is 4.7 μm for BT ceramics [20]. As observed by FE-SEM, C-BT and C-BT/Mn have sufficiently smaller grains compared to this critical grain size. In fact, the FE-SEM observation of chemically etched surface (Fig. 4) shows that C-BT/Mn has the simple lamellar type domain structure. The observed width of a single domain in C-BT/Mn is approximately 80 nm, which is consistent with that in a pure BT ceramic with a similar grain size (~ 0.5 μm) [21], indicating that the coating of BT particles with Mn-doped BT has no influence on the domain structure of the final sintered ceramic.

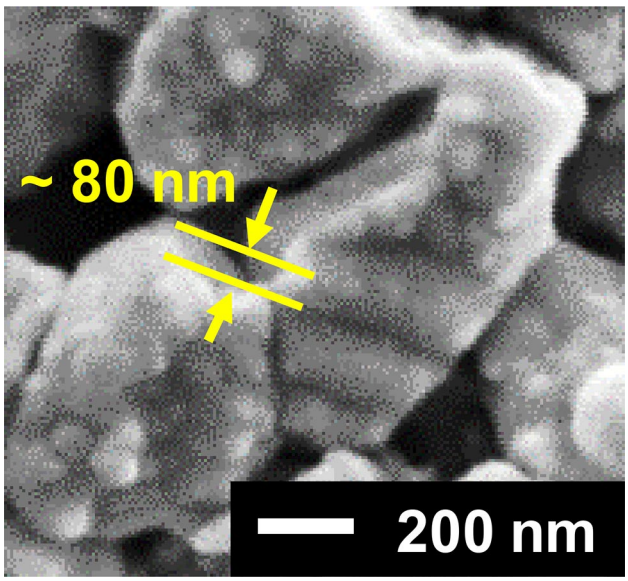

Fig. 4 An FE-SEM image of the surface of the chemically etched surface of C-BT/Mn. The yellow lines in the figure show the approximate width of a single domain (~ 80 nm)

Figure 5 compares XRD patterns of C-BT and C-BT/Mn. All diffraction peaks from both samples can be indexed to the tetragonal perovskite structure of BT, showing that there are no secondary phase in these samples. It is also observed that the coating with Mn-doped BT causes no change in the lattice parameters, and as a result, both samples show the same tetragonality *c*/*a* of 1.008. This *c*/*a* value is well consistent with the reported value for a pure BT ceramic with a grain size of 0.5 μm [22]. It has been reported that doping of Mn into BT at a concentration less than 1 mol % results in a slight decrease in *c*/*a* [23]. The observed unchanged *c*/*a* thus suggests that most part of C-BT/Mn is the pure BT phase.

It is also observed from the 002 and 200 diffraction peaks of the samples that there is a "bridge" between these peaks, which can be attributed to overlapping of the reflections from crystal lattices with smaller tetragonal distortions (i.e., $c/a < 1.008$). Here we compare the bridge height of C-BT and C-BT/Mn using the ratio of the intensities at the 200 peak (I_{200}) and at the center of the bridge (I_b). The I_{200}/I_b ratio is calculated to be 0.214 for C-BT, whereas C-BT/Mn show a higher I_{200}/I_b ratio of 0.225. One possible reason for the formation of such a bridge is the

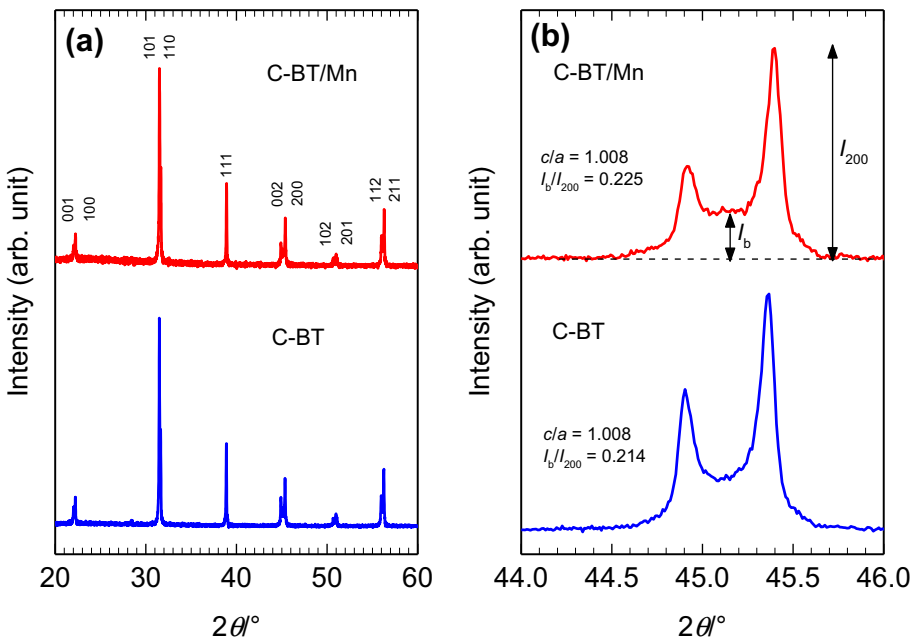

Fig. 5 **a** XRD patterns of C-BT and C-BT/Mn, and **b** magnified images of these profiles around the (002) and (200) diffraction peaks

90° domain walls: the crystal lattices near the 90° domain wall are strained to have a smaller *c*/*a*, and hence a sample with a higher domain wall density (number of domain walls per unit volume) show a higher bridge [17]. With regard to C-BT and C-BT/Mn, however, the difference in the bridge height between them should not be attributed to the difference in the domain wall density in these samples because they have a similar grain size, hence, a similar domain wall density. Thus we consider that the higher bridge in C-BT/Mn is caused by the doped Mn ions: the Mn ions in a C-BT/Mn grain are concentrated near grain boundaries, hence the *c*/*a* is unchanged inside the grain but decreased in the Mn-doped region, resulting in the observed unchanged overall *c*/*a* and the higher bridge.

Temperature dependence of ε_r was measured for C-BT and C-BT/Mn to check their T_C (Fig. 6). For comparison, the data for a BT ceramic homogeneously doped with 0.5 mol% Mn through the conventional solid-state route (hereafter referred to as "conventional hard BT") is also shown. All samples show a sharp peak attributed to tetragonal ferroelectric–cubic paraelectric phase transition. T_C determined by the dielectric peak is 123.9 °C and 122.2 °C for C-BT and C-BT/Mn, respectively. It is known that T_C of Mn-doped BT monotonically decreases with increasing the Mn content [24]. The conventional hard BT actually shows T_C at 117.0 °C, which is 6.9 °C lower than C-BT. With regard to C-BT/Mn, the overall Mn content in the sample is estimated to be 0.17 mol% from the amounts of raw materials used for the co-precipitation process. The observed T_C shift in C-BT/Mn is found small even considering the small Mn concentration in the sample. In this study we could not directly observe the spatial distribution of the Mn ions in C-BT/Mn by an elemental analysis because of the low concentration of the Mn ions. Nevertheless, the results of the structural and dielectric measurements shown above strongly suggest that Mn ions in C-BT/Mn are retained around grain boundary even after the sintering process to form a core–shell structure composed of the core of almost pure BT and the shell of Mn-doped BT.

Figure 7 shows room-temperature *S*—*E* curves of C-BT and C-BT/Mn. The data for the conventional hard BT is also shown again for comparison. The *S*—*E* curve of C-BT at room temperature shows a large hysteresis, indicating the significant contribution from the irreversible domain wall motion to the piezoelectric strain in this sample. The effective piezoelectric coefficient d^*_{33}, which is defined by $d^*_{33} = S_{max}/E_{max}$ using the maximum strain S_{max} at the maximum electric field E_{max}, is calculated as 230 pm·V^{-1} for C-BT, which is comparable to the reported d_{33} value of a BT ceramic with a similar grain size (~ 0.5 μm) to C-BT [22]. The conventional hard BT shows an *S*—*E* curve smaller hysteresis compared to C-BT. However, d^*_{33} of this material is also decreased to 198 pm·V^{-1}. This is because in this material both reversible and irreversible domain wall motions are limited by the Mn ions uniformly dispersed in each grain. In contrast with the conventional hard BT, C-BT/Mn shows an almost same d^*_{33} with C-BT, while its hysteresis is effectively decreased to a similar level to the Mn-doped BT. These results clearly indicate that in C-BT/Mn the irreversible motion is effectively suppressed, while the reversible motion inside the grains remains possible.

Figure 8 shows *S*—*E* curves of C-BT and C-BT/Mn measured at temperatures between room temperature and T_C. The hysteretic behavior of *S*—*E* curve for both samples is observed to change in a complex manner as temperature increases to approach T_C. To discuss the temperature

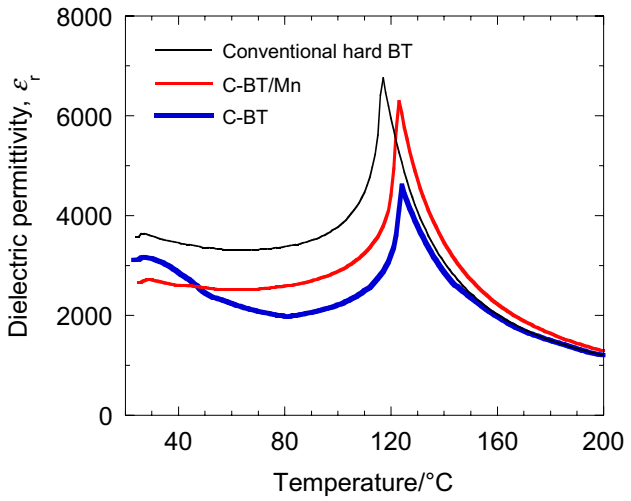

Fig. 6 Temperature dependence of dielectric permittivity of C-BT and C-BT/Mn. Data for the conventional hard BT (0.5 mol% Mn-doped) ceramic is also shown for comparison

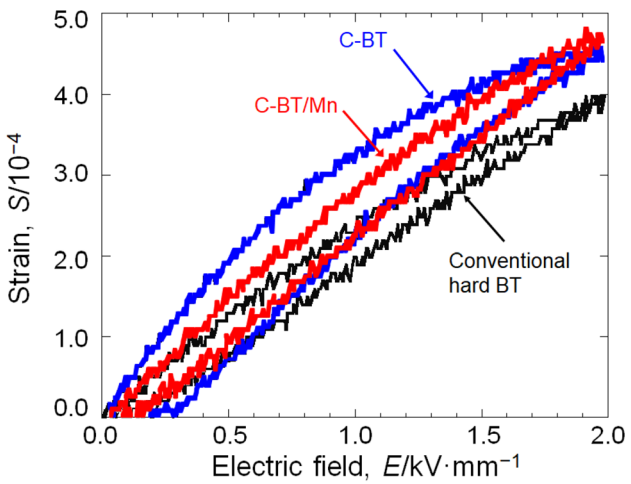

Fig. 7 Room-temperature *S*—*E* curves of C-BT and C-BT/Mn. Data for the conventional hard BT (0.5 mol% Mn-doped) ceramic is also shown for comparison

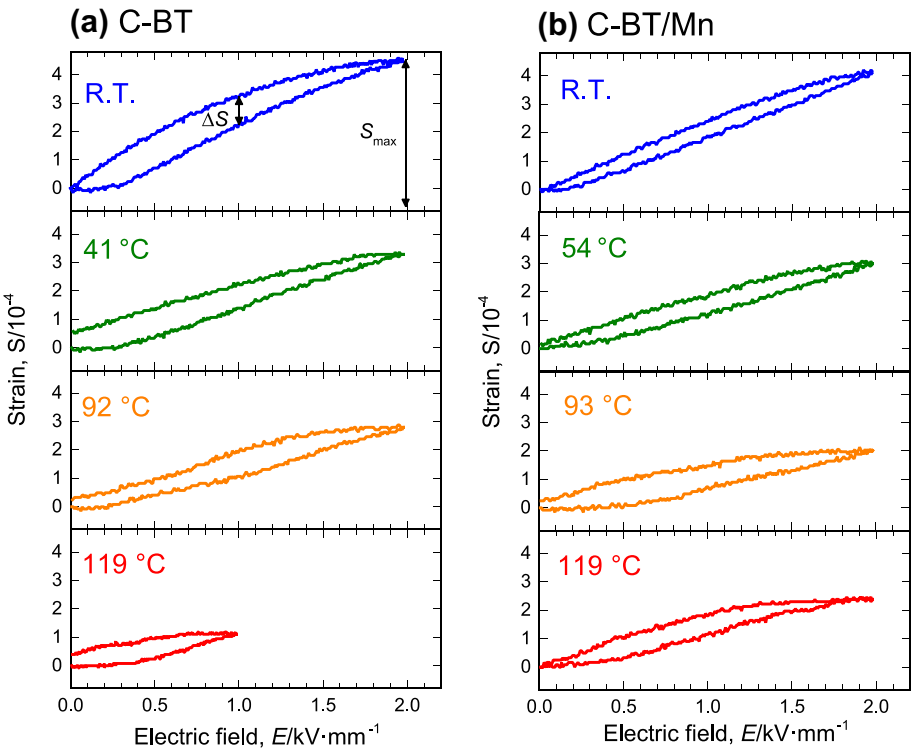

Fig. 8 *S*–*E* curves of **a** C-BT and **b** C-BT/Mn measured between room temperature and a temperature just below T_C

variation of hysteretic behavior of the ceramics quantitatively, we define the degree of hysteresis *H* as:

$$H = \Delta S/S_{max} \times 100\,(\%), \quad (1)$$

where ΔS is the difference between the strains at $E = E_{max}/2$ measured upon increasing and decreasing the field. Temperature dependences of d^*_{33} and *H* for C-BT and C-BT/Mn are shown in Fig. 9. Note that most measurements were performed at $E_{max} = 2.0$ kV·mm^{-1}, but for C-BT, the data above 100 °C was measured at $E_{max} = 1.0$ kV·mm^{-1} because dielectric breakdown occurred under the higher electric field. The plots measured at $E_{max} = 1.0$ kV·mm^{-1} are shown using blue triangles. A similar temperature dependence of d^*_{33} is found for both samples: d^*_{33} first decreases with temperature and then slightly increases at temperatures near T_C. This behavior can be explained from the temperature dependences of ε_r and polarization. Piezoelectric d_{33} coefficient is thermodynamically related to ε_r and remanent polarization (P_r) as:

$$d_{33} = 2\varepsilon_0\varepsilon_r Q P_r, \quad (2)$$

where ε_0 is permittivity of vacuum, *Q* is electrostrictive coefficient. Because *Q* is almost constant against temperature variation [25], the temperature dependence of d_{33} is determined by those of ε_r and P_r. Polarization of BT monotonically decreases as temperature approaches T_C. Thus d^*_{33} of the samples decreases with increasing temperature in the range between room temperature and 100 °C, where ε_r is almost constant or decreases (see Fig. 6). At temperatures just near but lower than T_C, ε_r drastically increases due to the phase transition to surpass the influence of the P_r decrease, resulting in a slight increase of d^*_{33}.

In contrast to d^*_{33}, *H* shows different temperature dependencies for C-BT and C-Bt/Mn. *H* of C-BT is almost constant (~ 23%) at temperatures below 80 °C and then drastically increases at higher temperatures. It should be noted again that the data above 100 °C for this sample was measured under a smaller E_{max} of 1.0 kV·mm^{-1}. In general the hysteresis behavior of unipolar *S*–*E* curve has a complex dependence on E_{max}; *H* of some materials decreases with E_{max}, while that of other materials increases. Such a behavior is related to the shape of the *S*–*E* curve. It is reported that *H* of $0.84Pb(Hf_{0.4}Ti_{0.6})O_3$–$0.16Pb(Yb_{0.5}Nb_{0.5})O_3$ piezoelectric ceramics, which show a normal S-shaped strain curve similar to C-BT, is less dependent on E_{max} [26]. Both samples studied here show S-shaped or linear *S*–*E* curves at all measuring temperatures, hence little E_{max} dependence of *H* is expected. To check the E_{max} dependence of *H* for C-BT, we performed the *S*–*E* measurement at room temperature (17 °C) at both E_{max} of 1.0 kV·mm^{-1} and 2.0 kV·mm^{-1}. As a result, we confirmed that *H* was almost constant at this E_{max} range as shown in Fig. 9b. This shows that the comparison among data plots measured under different E_{max} is reasonable. It is observed that C-BT/Mn does not show the sudden increase in *H* at temperatures near T_C. As a result, C-BT/Mn shows much smaller *H* values compared to C-BT at elevated temperatures. This behavior can be attributed to the Mn ions doped near the grain

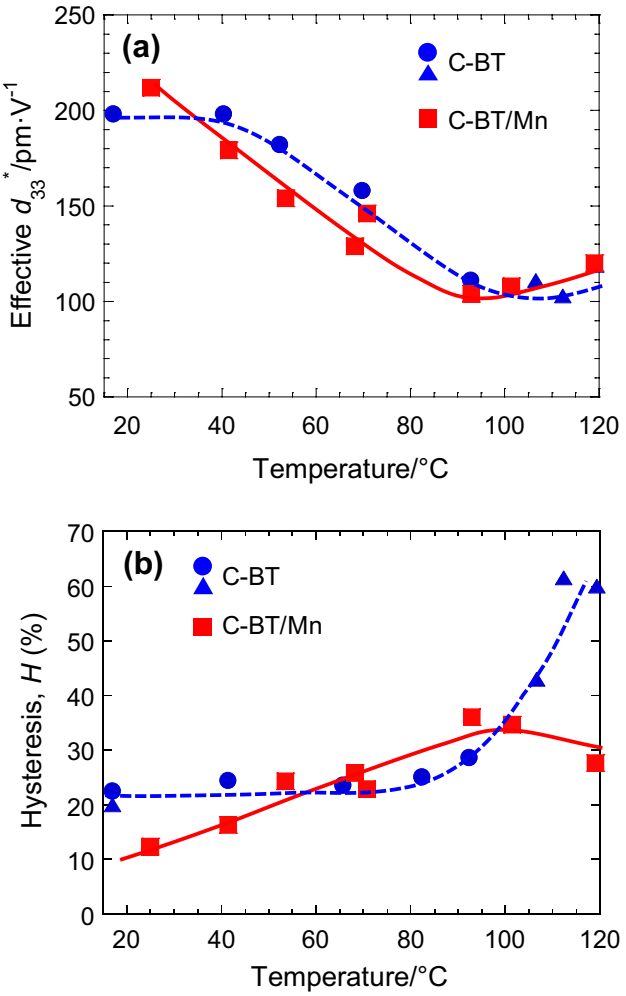

Fig. 9 Temperature dependence of **a** effective piezoelectric coefficient d_{33}^* and **b** hysteresis H for C-BT and C-BT/Mn. The data plots measured at 1.0 kV·mm^{-1} for C-BT were shown using filled triangles. The lines are shown as a guide to the eye

boundary. The Mn ions and oxygen vacancies effectively pin domain walls to suppress the irreversible domain wall motion at elevated temperatures, while they allow the reversible motion inside the grains, leading to the high d_{33}^* and suppressed H. We believe that such a control of the domain wall motion using localized acceptor ions is an effective way to develop piezoelectric ceramics suitable for the high-temperature actuator applications.

4 Conclusion

In this study, a Mn-modified BT ceramic was prepared by sintering of BT particles coated with Mn-doped BT. The XRD patterns and temperature dependence of dielectric permittivity indicated that the resulting BT ceramic have a core–shell structure composed of the undoped core and the Mn-doped shell. The measurement of unipolar piezoelectric strain curves showed that the increase in the hysteresis at temperatures near T_C was suppressed in the Mn-modified ceramic in comparison with the unmodified BT ceramic, whereas the effective piezoelectric coefficient d_{33}^* was comparable for both samples. The results indicate that the irreversible domain wall motion was effectively suppressed by the Mn ions localized near grain boundaries, while the reversible is not affected. The proposed method for controlling the domain wall mobility using inhomogeneously doped acceptors can lead to the development of novel high-temperature piezoelectric ceramics with a wider operation temperature range.

Funding This work was supported by a Grant-in-Aid for Research Activity Start-up (No. 25889049) from the Japan Society for the Promotion of Science (JSPS).

Compliance with ethical standards

Conflict of interest The authors declare that they have no conflict of interest.

References

1. Damjanovic D, Demartin M (1997) Contribution of the irreversible displacement of domain walls to the piezoelectric effect in barium titanate and lead zirconate titanate ceramics. J Phys Condens Matter 9:4943–4953. https://doi.org/10.1088/0953-8984/9/23/018
2. Tsurumi T, Sasaki T, Kakemoto H, Harigai T, Wada S (2004) Domain contribution to direct and converse piezoelectric effects of PZT ceramics. Jpn J Appl Phys 43:7618–7622. https://doi.org/10.1143/JJAP.43.7618
3. Bassiri-Gharb N, Fujii I, Hong E, Trolier-Mckinstry S, Taylor DV, Damjanovic D (2007) Domain wall contributions to the properties of piezoelectric thin films. J Electroceram 19:47–65. https://doi.org/10.1007/s10832-007-9001-1
4. Pramanick A, Damjanovic D, Daniels JE, Nino JC, Jones JL (2011) Origins of electro-mechanical coupling in polycrystalline ferroelectrics during subcoercive electrical loading. J Am Ceram Soc 94:293–309. https://doi.org/10.1111/j.1551-2916.2010.04240.x
5. Damjanovic D (1998) Ferroelectric, dielectric and piezoelectric properties of ferroelectric thin films and ceramics. Rep Prog Phys 61:1267–1324. https://doi.org/10.1088/0034-4885/61/9/002
6. Damjanovic D, Demartin M, Shulman HS, Testorf M, Setter N (1996) Instabilities in the piezoelectric properties of ferroelectric ceramics. Sens Actuators A 53:353–360. https://doi.org/10.1016/0924-4247(96)80160-9
7. Hall DA (2001) Nonlinearity in piezoelectric ceramics. J Mater Sci 36:4575–4601. https://doi.org/10.1023/A:1017959111402
8. Zheng J, Takahashi S, Yoshikawa S, Uchino K, de Vries JWC (1996) Heat generation in multilayer piezoelectric actuators. J Am Ceram Soc 79:3193–3198. https://doi.org/10.1111/j.1151-2916.1996.tb08095.x
9. Senousy MS, Rajapakse RKND, Mumford D, Gadala MS (2009) Self-heat generation in piezoelectric stack actuators used

in fuel injectors. Smart Mater Struct 18:045008. https://doi.org/10.1088/0964-1726/18/4/045008
10. Randall CA, Kelnberger A, Yang GY, Eitel RE, Shrout TR (2005) High strain piezoelectric multilayer actuators—a material science and engineering challenge. J Electroceram 14:177–191. https://doi.org/10.1007/s10832-005-0956-5
11. Eitel RE, Randall CA, Shrout TR, Park SE (2002) Preparation and characterization of high temperature perovskite ferroelectrics in the solid-solution $(1-x)BiScO_3$–$xPbTiO_3$. Jpn J Appl Phys 41:2099–2104. https://doi.org/10.1143/JJAP.41.2099
12. Algueró M, Ramos P, Jiménez R, Amorín H, Vila E, Castro A (2012) High temperature piezoelectric $BiScO_3$–$PbTiO_3$ synthesized by mechanochemical methods. Acta Mater 60:1174–1183. https://doi.org/10.1016/j.actamat.2011.10.050
13. Haertling GH (1999) Ferroelectric ceramics: history and technology. J Am Ceram Soc 82:797–818. https://doi.org/10.1111/j.1151-2916.1999.tb01840.x
14. Robels U, Arlt G (1993) Domain wall clamping in ferroelectrics by orientation of defects. J Appl Phys 73:3454–3460. https://doi.org/10.1063/1.352948
15. Yang TJ, Gopalan V, Swart PJ, Mohideen U (1999) Direct observation of pinning and bowing of a single ferroelectric domain wall. Phys Rev Lett 82:4106–4109. https://doi.org/10.1103/PhysRevLett.82.4106
16. Yoon D, Lee B, Badheka P, Wang X (2003) Barium ion leaching from barium titanate powder in water. J Mater Sci 4:165–169. https://doi.org/10.1023/A:1022306024907
17. Hoshina T, Takizawa K, Li J, Kasama T, Kakemoto H, Tsurumi T (2008) Domain size effect on dielectric properties of barium titanate ceramics. Jpn J Appl Phys 47:7607–7611. https://doi.org/10.1143/JJAP.47.7607
18. Chen IW, Wang XH (2000) Sintering dense nanocrystalline ceramics without final-stage grain growth. Nature 404:168–171. https://doi.org/10.1038/35004548
19. Zhao X, Chen W, Zhang L, Gao J, Zhong L (2015) Effect of fabrication routes on the microstructure, the dielectric and ferroelectric properties of the Mn-doped $BaTiO_3$ ceramics. Appl Phys A 118:931–938. https://doi.org/10.1007/s00339-014-8816-2
20. Arlt G (1990) Twinning in ferroelectric and ferroelastic ceramics: stress relief. J Mater Sci 25:2655–2666. https://doi.org/10.1007/BF00584864
21. Hoshina T (2013) Size effect of barium titanate: fine particles and ceramics. J Ceram Soc Jpn 121:156–161. https://doi.org/10.2109/jcersj2.121.156
22. Huan Y, Wang X, Fang J, Li L (2014) Grain size effect on piezoelectric and ferroelectric properties of $BaTiO_3$ ceramics. J Eur Ceram Soc 34:1445–1448. https://doi.org/10.1016/j.jeurceramsoc.2013.11.030
23. Kirianov A, Ozaki N, Ohsato H, Kohzu N, Kishi H (2001) Studies on the solid solution of Mn in $BaTiO_3$. Jpn J Appl Phys 40:5619–5623. https://doi.org/10.1143/JJAP.40.5619
24. Ihrig H (1978) The phase stability of $BaTiO_3$ as a function of doped 3d elements: an experimental study. J Phys C Solid State Phys 11:819–827. https://doi.org/10.1088/0022-3719/11/4/026
25. Uchino K, Nomura S, Cross LE, Newnham RE, Jang SJ (1981) Electrostrictive effect in perovskites and its transducer applications. J Mater Sci 16:569–578. https://doi.org/10.1007/BF00552193
26. Tang H, Zhang S, Feng Y, Li F, Shrout TR (2013) Piezoelectric property and strain behavior of $Pb(Yb_{0.5}Nb_{0.5})O_3$–$PbHfO_3$–$PbTiO_3$ polycrystalline ceramics. J Am Ceram Soc 96:2857–2863. https://doi.org/10.1111/jace.12389